International Journal for Parasitology: Drugs and Drug Resistance 25 (2024) 100545

Contents lists available at ScienceDirect

International Journal for Parasitology: Drugs and Drug Resistance

journal homepage: www.elsevier.com/locate/ijpddr

Exploring therapeutic approaches against *Naegleria fowleri* infections through the COVID box

Javier Chao-Pellicer [a,b,c], Iñigo Arberas-Jiménez [a,b], Ines Sifaoui [a,b,c], José E. Piñero [a,b,c,*], Jacob Lorenzo-Morales [a,b,c,**]

[a] Instituto Universitario de Enfermedades Tropicales y Salud Pública de Canarias, Universidad de La Laguna, Avda. Astrofísico Fco. Sánchez, S/N, 38203, San Cristóbal de La Laguna, Spain

[b] Departamento de Obstetricia y Ginecología, Pediatría, Medicina Preventiva y Salud Pública, Toxicología, Medicina Legal y Forense y Parasitología, Universidad de La Laguna, 38203, San Cristóbal de La Laguna, Spain

[c] Centro de Investigación Biomédica en Red de Enfermedades Infecciosas (CIBERINFEC), Instituto de Salud Carlos III, 28220, Madrid, Spain

ARTICLE INFO

Keywords:
Naegleria fowleri
Primary amoebic meningoencephalitis
Chemotherapy
COVID box
Programmed cell death

ABSTRACT

Naegleria fowleri, known as the brain-eating amoeba, is the pathogen that causes the primary amoebic meningoencephalitis (PAM), a severe neurodegenerative disease with a fatality rate exceeding 95%. Moreover, PAM cases commonly involved previous activities in warm freshwater bodies that allow amoebae-containing water through the nasal passages. Hence, awareness among healthcare professionals and the general public are the key to contribute to a higher and faster number of diagnoses worldwide. Current treatment options for PAM, such as amphotericin B and miltefosine, are limited by potential cytotoxic effects. In this context, the repurposing of existing compounds has emerged as a promising strategy. In this study, the evaluation of the COVID Box which contains 160 compounds demonstrated significant in vitro amoebicidal activity against two type strains of *N. fowleri*. From these compounds, terconazole, clemastine, ABT-239 and PD-144418 showed a higher selectivity against the parasite compared to the remaining products. In addition, programmed cell death assays were conducted with these four compounds, unveiling compatible metabolic events in treated amoebae. These compounds exhibited chromatin condensation and alterations in cell membrane permeability, indicating their potential to induce programmed cell death. Assessment of mitochondrial membrane potential disruption and a significant reduction in ATP production emphasized the impact of these compounds on the mitochondria, with the identification of increased ROS production underscoring their potential as effective treatment options. This study emphasizes the potential of the mentioned COVID Box compounds against *N. fowleri*, providing a path for enhanced PAM therapies.

1. Introduction

The genus Naegleria, comprising 47 species (De Jonckheere, 2011), includes the species *Naegleria fowleri*, commonly known as the brain-eating amoeba. The surge in the number of reported cases, coupled with increased public awareness, has brought this microorganism into prominence due to its pathogenic capacity to induce a CNS infection known as primary amoebic meningoencephalitis (PAM) (Güémez and García, 2021).

PAM is a rare disease, with a fatality rate of over 90% (Jahangeer et al., 2020). Furthermore, individuals who are most susceptible to PAM are often engaged in activities involving water sports or recreational activities in warm freshwater bodies, leading to water inhalation through the nasal passages (Cope et al., 2015; Kemble et al., 2012; Linam et al., 2015). In addition, PAM primarily affects young children, adolescents, and young adults, and it is crucial to recognize the early symptoms of the disease for timely intervention (Martínez et al., 2022).

As mentioned above, infection usually begins with the inhalation of

* Corresponding author. Instituto Universitario de Enfermedades Tropicales y Salud Pública de Canarias, Universidad de La Laguna, Avda. Astrofísico Fco. Sánchez, S/N, 38203, San Cristóbal de La Laguna, Spain.

** Corresponding author. Instituto Universitario de Enfermedades Tropicales y Salud Pública de Canarias, Universidad de La Laguna, Avda. Astrofísico Fco. Sánchez, S/N, 38203, San Cristóbal de La Laguna, Spain.

E-mail addresses: jchaopel@ull.edu.es (J. Chao-Pellicer), iarberas@ull.edu.es (I. Arberas-Jiménez), isifaoui@ull.edu.es (I. Sifaoui), jpinero@ull.edu.es (J.E. Piñero), jmlorenz@ull.edu.es (J. Lorenzo-Morales).

https://doi.org/10.1016/j.ijpddr.2024.100545
Received 26 February 2024; Received in revised form 25 April 2024; Accepted 30 April 2024
Available online 7 May 2024
2211-3207/© 2024 The Authors. Published by Elsevier Ltd on behalf of Australian Society for Parasitology. This is an open access article under the CC BY-NC-ND license (http://creativecommons.org/licenses/by-nc-nd/4.0/).

the trophozoite or cyst stages, present in water bodies or wet soils. Upon reaching the individual's nasal mucosa, if they are in the cyst form, these transform into the trophozoite stage (Piñero et al., 2019), establishing a neurochemical gradient due to exposure to specific chemical substances. This is a result of their chemoattraction to neurotransmitters associated with brain neurons, such as acetylcholine or noradrenaline (Baig, 2016). Consequently, their locomotion is triggered, causing damage along the path towards the brain, which, in advanced stages, greatly diminishes the patient's chances of survival. These injuries result from the release of cysteine proteases by the amoeba, causing irreversible damage (Lee et al., 2014; Serrano-Luna et al., 2007). These proteases play essential roles in either invading host tissues or evading the immune system, thus promoting the disease's progression (Rodríguez-Mera et al., 2022). Therefore, leading to the onset of symptoms. In its early stages, patients may experience non-specific encephalitis symptoms such as headaches, fever, and nausea, often mistaken as viral infections. However, as the disease progresses, more severe neurological manifestations emerge, including altered mental status, seizures, and hallucinations. PAM rapid evolution leads to a significant decline in the patient's condition, with a propensity towards coma, often followed by a fatal outcome (Grace et al., 2015; Güémez and García, 2021).

The diagnosing of *N. fowleri* infection is a significant challenge due to its low morbidity and rapid progression. Commonly, methods like cerebrospinal fluid analysis, induction of the flagellar or cyst stage, Polymerase Chain Reaction (PCR), and neuroimaging techniques are employed to confirm the parasite's presence and evaluate associated damage (Grace et al., 2015; Schumacher et al., 1995). However, an early diagnosis is crucial for effective treatment, emphasizing the need for greater awareness among healthcare professionals and better diagnostic tools to improve detection and patient outcomes, in view of the limited number of diagnosed cases.

Currently, there are no specific drugs exclusively designed to fight this infection. The treatment approaches often rely on a combination of medications such as amphotericin B and miltefosine, along with certain azole drugs that have demonstrated synergistic activity (Bellini et al., 2018; Dunnebacke et al., 2004; Linam et al., 2015; Schuster et al., 2006). Furthermore, adjunctive neuroprotective strategies have been explored, including the induction of hypothermia and the administration of corticosteroids such as dexamethasone, among others, are implemented (Dunn et al., 2016; Heggie and Küpper, 2017; Jain et al., 2002). While these therapies aim to combat the parasite, it is important to note that many of these medications are metabolized in vital organs and possess cytotoxic properties. This raises concerns about potential organ damage as a result of the treatment itself, adding an additional layer of complexity to managing this devastating disease (Laniado-Laborín and Cabrales-Vargas, 2009). As a result, research efforts continue to explore more targeted and effective treatment options to improve patient outcomes and minimize potential side effects.

In the search for new therapeutic agents, an effective strategy involves repositioning existing compounds, a method that is both cost-effective and time-saving (Chang et al., 2015; Pushpakom et al., 2019). This approach gains particular significance in the current global context, with the world grappling with the COVID-19 pandemic, which has propelled the search for potent antiviral agents. Initiatives such as the COVID Box have surfaced in response to this pressing demand, offering a curated collection of 160 potential drug candidates (Almeida--Paes et al., 2021). These compounds encompass a range of bioactivities, each demonstrating activity or suspected activity against SARS-CoV-2, the virus responsible for the ongoing pandemic. Notably, these compounds have displayed promising biological activities not only in the fight against SARS-CoV-2 but also against other infectious agents, including parasitic protozoa (Abbaali et al., 2021; Almeida-Paes et al., 2021; El Saftawy et al., 2024; Reigada et al., 2019). As the demand for innovative treatments against the deadly *N. fowleri* pathogen intensifies, exploring the potential of COVID Box compounds to address this amoebic infection emerges as a highly auspicious avenue for research. This article delves into the potential efficacy of these compounds in targeting *N. fowleri*, offering a new and promising path in the ongoing battle against PAM.

2. Material and methods

2.1. Chemicals

The COVID Box, provided by Medicines for Malaria Venture (MMV, Geneva, Switzerland), is a collection of 160 commercially available drugs with known or predicted activity against the newly discovered pandemic virus, SARS-CoV-2, as shown in Supplemental Materials S1. These compounds are initially arranged in 96-well plates at a concentration of 10 mM, which are diluted to a concentration of 1 mM using dimethyl sulfoxide (DMSO) for testing against *N. fowleri*. DMSO was not exceeded at 1% of the total volume to avoid toxic effects on the parasites.

After a first screening, four pure compounds were purchased. Terconazole was obtained from Cymit Química S.L. (Barcelona, Spain). ABT-239 and PD-144418 were purchased from MedChemExpress (Monmouth Junction, NJ, USA). Clemastine was purchased from Sigma-Aldrich (Madrid, Spain).

2.2. Amoebic and cell culture

In the present study, two clinical strains were used to evaluate the sensitivity of the compounds obtained from the COVID Box. Both strains, ATCC® 30,808™ (Strain KUL, obtained from Belgium) and ATCC® 30,215™ (Strain Nf69, obtained from Australia), were acquired from the American Type Culture Collection (ATCC) and selected for this research. The strains were maintained in axenic trophozoite stage in culture flask grown in 2% Bactocasitone medium, supplemented with 10% (v/v) fetal bovine serum (FBS) (Biowest, VWR, Barcelona, Spain), 0.3% penicillin G sodium salt (Sigma-Aldrich, Madrid, Spain), and 0.5 mg/mL streptomycin sulphate (Sigma-Aldrich, Madrid, Spain). To be maintained at this stage, the culture was incubated at 37 °C. On the other hand, to induce the cyst stage, the trophozoites were cultured in MYAS medium at 28 °C together with agitation on an orbital shaker. Under these conditions, the trophozoites underwent a transformation into the resistant stage of the parasite in approximately 10 days, as described in the protocol published by Arberas-Jiménez et al. (2022); Arberas-Jiménez et al. (2022).

Amoebae cultures were handled in a biosafety level 3 (BSL-3) laboratory, provided at the Instituto Universitario de Enfermedades Tropicales y Salud Pública de Canarias, University of La Laguna, following the explicit list provided in Real Decreto 664/1997 of May 12, 1997, which is designed to safeguard the well-being of workers against potential hazards associated with their exposure to biological agents during their work activities.

In cytotoxicity assessments, the compounds were subjected to evaluation using a murine macrophage cell line, J774A.1 (ATCC® TIB-67™), maintained in Dulbecco's modified Eagle's medium (DMEM, w/v) supplemented with 10% (v/v) FBS and 10 μg/mL gentamicin (Sigma-Aldrich, Madrid, Spain). To promote optimal growth, the cultures were incubated in a controlled environment, precisely at 37 °C with a 5% CO_2 concentration.

2.3. In vitro activity against trophozoites and cysts of N. fowleri

The screening of the 160 compounds was conducted. *N. fowleri* trophozoites (ATCC® 30,808™ strain) were seeded at a concentration of 2 $\times$ 10^5 cells/mL in Bactocasitone culture medium using a Countess 3 FL Automated Cell Counter (Thermo Fisher Scientific, Spain). The trophozoites were allowed to adhere to the plate for 15 min. Afterward, the compounds were added at a concentration of 100 μM, with each occupying one well of the plate. After the addition, the alamarBlue® reagent was placed, enabling the selection of relevant compounds through a

colorimetric change. The compounds that did not meet the specified activity criteria or exhibited cytotoxicity above predetermined thresholds were excluded. Specifically, compounds that achieved both a 60% inhibition of the amoebic population and less than 20% cytotoxicity when cultured with macrophages were selected for further studies.

To evaluate the in vitro activity of the selected compounds, chemotherapy assays were performed in 96-well plates. In short, *N. fowleri* trophozoites (at the same concentration mentioned above) were added. Once the trophozoites were incubated, the previously diluted compounds (DMSO) were added to the plate. Negative control cells were incubated with bactocasitone medium alone. Finally, a 10% of the total volume of alamarBlue® was added. After 48 h of incubation, the EnSpire® Multimode Plate Reader (PerkinElmer, Madrid, Spain) was used to measure the emitted fluorescence (McBride et al., 2005; Rizo-Liendo et al., 2019) at 570/585 nm. To determine the Inhibitory concentrations 50 and 90 values, a nonlinear regression analysis with a 95% confidence interval was conducted using GraphPad Prism 9 software.

Following the evaluation of the molecule's activity on *N. fowleri* trophozoites, the same experiment was performed against the cyst stage. For this purpose, *N. fowleri* cysts were initially pre-treated with 1% SDS to eliminate any non-mature cysts. Afterward, to assess the efficacy of the chemicals against the parasite's resistant phase, serial dilutions were prepared in a 96-well microtiter plate (Thermo Fisher Scientific, Madrid, Spain). Once the compounds were diluted, 2×10^5 cells/mL of *N. fowleri* cysts were incubated. After the 24-h cyst incubation, the growth medium of the 96-well plate was replaced to facilitate excystation and determine cyst viability. Non-treated *N. fowleri* cysts were used as the negative control. Subsequently, alamarBlue® cell viability reagent (10% of the well total volume) was added, enabling to differentiate between non-viable cysts and trophozoites by oxidation-reduction reactions. After, the activity plates were incubated at 37 °C for 72 h. Fluorescence values were obtained using the EnSpire® Multimode Plate Reader (PerkinElmer, Madrid, Spain), and the IC_{50} was determined from statistical analysis.

2.4. In vitro cytotoxicity against murine macrophages cell line

For the evaluation of cytotoxicity of the products of interest, a murine macrophage cell line J774A.1 (ATCC® TIB-67™) was used. The macrophages were cultured in 96-well plates at a concentration of 10^5 cells/mL using the Countess 3 FL Automated Cell Counter (Thermo Fisher Scientific, Spain) with RPMI (Roswell Park Memorial Institute, 1640) medium supplemented with 10% fetal bovine serum at 37 °C in a 5% CO_2 atmosphere. Subsequently, the diluted compounds were added at different concentrations. Finally, 10% of the total volume of alamarBlue® was added as previously mentioned. The plate was read using an EnSpire® Multimode Plate Reader (PerkinElmer, Madrid, Spain) and analyzed in GraphPad Prism 9.0 to determine the cytotoxic concentration (CC_{50}) and subsequently obtain the selectivity index (CC_{50}/IC_{50}).

2.5. Programmed cell death (PCD) induction in N. fowleri

A selection of the products of relevance, those with the highest selectivity index, was used to study programmed cell death (PCD) in *N. fowleri* (ATCC® 30,808™). Therefore, the trophozoites were incubated in a 96-well plate at a concentration of 5×10^5 cells/mL making use of a Countess 3 FL Automated Cell Counter (Thermo Fisher Scientific, Spain). Once attached to the wells, they were treated with IC_{90} of the chemicals during 24 h. In order to expose the different metabolic events characteristic of a PCD, the reagents were added according to manufacturer's instructions under dark conditions to avoid their degradation. The results were revealed by fluorescence obtained using EVOS™ M5000 fluorescence inverted microscope (Invitrogen, Thermo Fisher Scientific, Madrid, Spain). For each objective lens thickness (40 × and 100 ×), five images were taken. The percentage of stained cells after the incubation of the cells with the dyes was also calculated. Moreover, a one-way analysis of variance (ANOVA) was used for data analysis on order to evaluate the differences between negative control and treated cells. The results are shown as the mean value of three different images ± standard deviation (SD).

2.5.1. Analysis of chromatin condensation

To detect chromatin condensation, a double DNA-binding dyes named Hoechst 33,342/Propidium Iodide (PI) (Life Technologies, Madrid, Spain) and an inverted fluorescence microscope EVOS™ FL Cell Imaging System M5000 (Life Technologies, USA) were used. To perform the experiment, the fluorescent reagents were added at a final concentration of 1 μM for 15 min to amoebae previously treated for 24 h with the IC_{90} of the compounds. Double staining revealed three groups in the experiment: amoebae in PCD process emitting blue fluorescence due to chromatin staining; amoebae emitting blue and red fluorescence at the same time, indicating an advanced stage in the PCD pathway; and no fluorescence at all, which are the cells not treated with the compounds.

2.5.2. Plasma membrane permeability

During apoptosis, the cell membrane has the potential to become more permeable, leading to the release of specific molecules and triggering signaling pathways that culminate in controlled cell degradation. The plasma membrane integrity of non-treated and treated amoebae was evaluated using the DNA-binding dye SYTOX™ Green and the EVOS™ FL Cell Imaging System M5000 microscope (Life Technologies, USA) to reveal the presence of fluorescence. SYTOX™ Green reagent was added to a final concentration of 1 μM. Once added, the 96-well plate was left to incubate in the dark for 15 min. After this time, the results were detected under the inverted fluorescence microscope.

2.5.3. Assessment of mitochondrial membrane potential ($\Delta\Psi m$) depolarization

Assessment of the mitochondrial membrane potential of amoebae was performed using the JC-1 mitochondrial membrane potential detection kit (Cayman Chemicals Vitro SA, Madrid, Spain). After the incubation period of the amoebae with the compounds, 10 μl of JC-1 was added and incubated for 1 h. Due to the extended incubation period, trophozoites undergo morphological changes, displaying increased swelling. This agent emits fluorescence at two different wavelengths. When the mitochondrial membrane potential is in optimal conditions, the reagent will be found in dimer form in the mitochondria emitting red fluorescence (~590 nm). In contrast, mitochondrial damage will result in a decrease of this potential, causing the reagent to disperse and remain as a monomer emitting green fluorescence (~529 nm). In this assay, the fluorescence emitted by the dimer and the monomeric forms of the dye were measured using the EVOS™ M5000 Cell Imaging System software (Life Technologies, Madrid, Spain) in order to calculate the ratio between the red and the green fluorescence intensities. For this, three different images were analyzed and the mean value and the SD were determined. A decrease in the mentioned ratio of the treated cells when compared to the negative control indicates mitochondrial membrane damage.

2.5.4. Detection of amoebic ATP synthesis

To analyze the ATP levels of amoebae, the Cell Titter-GLO® Luminescent Cell Viability reagent (Promega Biotech Ibérica, Madrid, Spain) was used. Following the 24-h incubation, the same amount of reagent (v/v) was added as the volume of the plate. After addition of the reagent, the luminescence emitted was analyzed using the EnSpire® Multimode Plate Reader (PerkinElmer, Madrid, Spain).

2.5.5. Identification of intracellular ROS overproduction

During apoptosis, ROS can act as signals to trigger and regulate various cellular signaling pathways. Additionally, excessive accumulation of these can damage key components such as DNA, proteins, or lipids. The fluorogenic reagent CellROX® Deep Red (Invitrogen, Thermo

Fisher Scientific, Madrid, Spain) was used to determine the presence of reactive oxygen species (ROS). After incubation time with the compounds, the reagent was added at a final concentration of 5 mM for 30 min. This dye binds to the ROS and emits an intense red fluorescence.

2.6. Statistical analysis

The experiments in this study were performed in triplicate (n = 3), and statistical parameters including the mean and standard deviation (SD) were obtained. GraphPad Prism 9.0 (GraphPad Software, CA, USA) was utilized for generating inhibition curves and conducting statistical analyses. Differences between the values were assessed using one-way analysis of variance (ANOVA). The data are presented as mean ± standard deviation (SD) of the triplicate experiments, with a significance level set at $p < 0.05$.

3. Results

3.1. Screening of compounds from the COVID box library

For the initial screening of the COVID Box, the compounds demonstrating an amoebicidal activity against *N. fowleri* ATCC® 30,808™ trophozoites were highlighted (Fig. 1). As a result, 62 out of the 160 compounds were excluded and are not shown in the graph due to the absence of growth inhibition. Hence, 98 of the 160 molecules met this threshold; with 37 compounds that induced an inhibition between 60 and 80%, and 8 compounds that exhibited an inhibition exceeding 80%. However, this activity needs to be accompanied by low cytotoxicity. 33 compounds exhibited a cytotoxicity of less than 20% of the macrophage population. 14 of these compounds were selected, exhibiting amoebic inhibition percentages above 60% and cytotoxicity values below 20%. Among them, products which activity against *N. fowleri* had already been described and others not available on the market were excluded. The terconazole, clemastine, ABT-239 and PD-144418 were the selected molecules for further studies.

3.2. Demonstration of the inhibitory and cytotoxic effect of the COVID box compounds

The four selected molecules from the COVID Box were evaluated for their amoebicidal activity against the trophozoite form of two type strains of *N. fowleri*, ATCC® 30,808™ and ATCC® 30,215™. Simultaneously, their toxicity was assessed using the murine macrophage cell line J774A.1 (ATCC® TIB-67). Activity assays revealed that out of the tested compounds, four of them exhibited significant activity, as presented in Table 1. Specifically, terconazole, clemastine, ABT-239 and PD-144418 (Fig. 2) demonstrated remarkable amoebicidal activity (Table 1) with low toxicity. Out of these four products, terconazole demonstrated significant anti-*Naegleria* activity, exhibiting consistent IC_{50} values against ATCC® 30,808™ and ATCC® 30,215™ strains (3.68 ± 0.61 μM and 0.81 ± 0.49 μM, respectively). Moreover, this molecule demonstrated the least cytotoxicity among the selected compounds, with a CC_{50} of 84.60 ± 15.58 μM, indicating its high selectivity and preference for the parasite. Furthermore, all compounds demonstrated cysticidal activity against *N. fowleri* with IC_{50} values ranging from 2.46 to 10.44 μM.

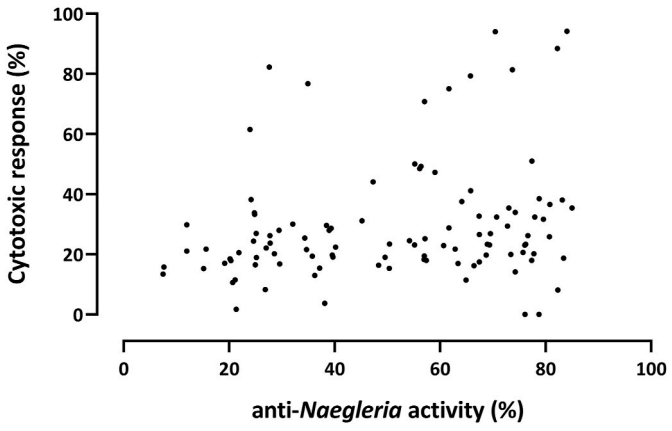

Fig. 1. Scatter plot representing the amoebic growth inhibition (%) and cytotoxic effect (%) of the screening of the 98 molecules. Only those demonstrating a certain amoebic inhibition were included in the data graph.

3.3. Programmed cell death process induced in N. fowleri

The four previously mentioned compounds were used to study the type of PCD observed in *N. fowleri*. To evaluate, trophozoites of ATCC® 30,808™ strain were treated with the IC_{90} of the molecules for 24 h. Non-treated amoebae were used as a negative control in each experiment, while amphotericin B served as a positive reference for evaluating PCD process.

3.3.1. Alterations in chromatin structure

The chromatin condensation, a characteristic indicator of cell death, was analyzed using the Hoechst 33,342 stain (Life Technologies, Madrid, Spain), which binds to condensed chromatin emitting blue fluorescence. Additionally, the propidium iodide (PI) dye was also employed in the assay, binding to the DNA of cells in an advanced state of cell death, emitting red fluorescence. The results of this experiment demonstrated clear chromatin condensation, emitting blue fluorescence in treated amoebae with the selected compounds from the COVID Box (Fig. 3 E, H, K, N). Furthermore, none of the treatments resulted in the amoebae reaching an advanced stage of apoptosis, evidenced by the absence of red fluorescence (Fig. 3 F, I, L, O). These results could be contrasted with the controls employed. In the negative control (Fig. 3A–C), there is an absence of fluorescence due to the healthy state of the amoebae. In contrast, in those treated with amphotericin B (Fig. 3P–R), our reference drug, the emission of blue fluorescence was observed. Differences between the values were assessed using an ANOVA. The results displayed significant differences (****$p < 0.0001$) when comparing treated cells to the negative controls.

3.3.2. Cell membrane permeability shifts

To assess the increased membrane permeability caused by the COVID Box products, SYTOX™ Green (Life Technologies, Madrid, Spain) dye was employed. Similar to the COVID Box compound-treated samples (Fig. 4C–J), which seem to damage the plasma membrane, thus enhancing permeability, trophozoites treated with amphotericin B (Fig. 4 K, L), used as a positive control, emitted green fluorescence. Negative control (untreated) amoebae (Fig. 4 A, B) are impermeable to the reactive, resulting in non-fluorescence emission. This reagent targets the same cellular component as PI, binding to nucleic acids and causing fluorescence emission. However, SYTOX™ Green exhibits greater sensitivity and efficacy in the analysis of the cell membrane permeability. This explains the green fluorescence emitted upon the addition of this reagent in Fig. 4, contrasting the absence of red fluorescence in the previous assay using PI (Fig. 3). A one-way analysis of variance (ANOVA) was conducted to analyze disparities between the values, demonstrating significant divergences (****$p < 0.0001$) between the treated cells and the negative control.

3.3.3. Evaluation of mitochondrial membrane potential disruption

The disruption of mitochondrial membrane potential was determined using the JC-1 Mitochondrial Membrane Potential Detection Kit (Cayman Chemicals Vitro SA, Madrid, Spain). In this assay, emphasis is placed on the difference in intensity emitted between non-treated and treated trophozoites. Under normal conditions, as seen in the negative control (Fig. 5A–C), the reagent is in the form of J-aggregates emitting

Table 1
Antiparasitic response (equal to IC_{50}) of tested compounds against the two strains of *N. fowleri*, along with the assessment of the cytotoxic concentration (CC_{50}) in murine macrophages and their selectivity index (SI). Moreover, the IC_{90}s, used for programmed cell death assays in *N. fowleri* ATCC® 30,808™, are indicated. All data were obtained from the mean of the 3 replicates of each assay, with their corresponding standard deviation.

COMPOUND	*N. FOWLERI* ATCC® 30,808™ IC_{50} (MM)		*N. FOWLERI* ATCC® 30,215™ IC_{50} (MM)	MURINE MACROPHAGES J774.A1 CC_{50} (MM)	S.I. ATCC® 30,808™	*N. FOWLERI* ATCC® 30,808™ IC_{90} (MM)
	Trophozoite Stage	Cyst Stage				
TERCONAZOLE	3.68 ± 0.61	2.46 ± 0.28	0.81 ± 0.49	84.6 ± 15.58	22.99	30.91 ± 2.38
CLEMASTINE	7.68 ± 0.32	8.2 ± 3.37	5.69 ± 1.16	58.66 ± 3.88	7.64	18.56 ± 5.64
ABT-239	3.65 ± 0.79	9.41 ± 2.63	3.05 ± 0.2	68.5 ± 13.26	18.77	14.69 ± 4.09
PD-144418	4.71 ± 0.95	10.44 ± 2.3	6.48 ± 2.83	48.76 ± 12.5	10.35	17.35 ± 3.28
AMPHOTERICIN B	0.12 ± 0.03	0.53 ± 0.03	0.16 ± 0.02	≥200	≥1650	0.35 ± 0.02
MILTEFOSINE	38.74 ± 4.23	21.52 ± 2.62	81.57 ± 7.23	127.89 ± 8.85	3.3	89.47 ± 17.37

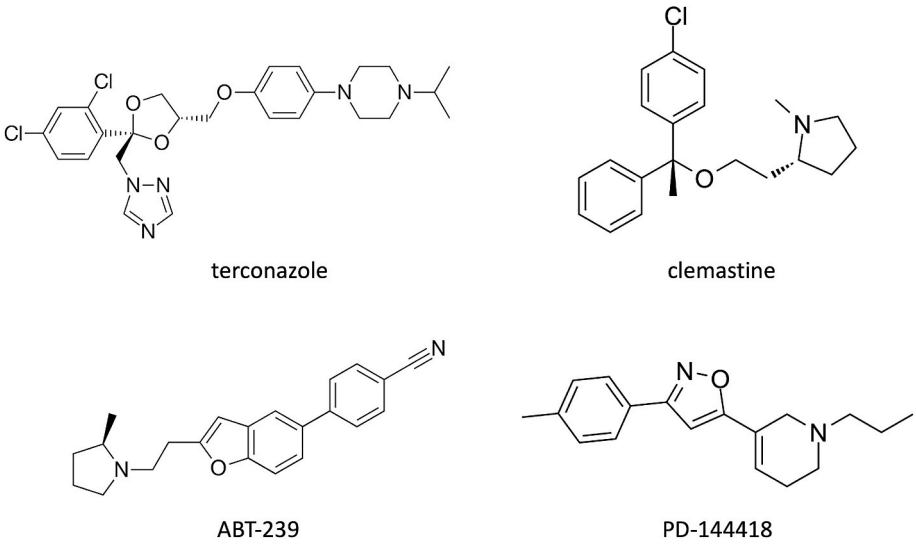

Fig. 2. 2D chemical structures of selected molecules.

red fluorescence due to the positive charge in this organelle. In contrast, amoebae exposed to the compounds (Fig. 5D–R) exhibit a drastic decrease in this potential, resulting in lower red colour intensity compared to healthy cells, causing the reagent to disperse and remain in a monomeric form emitting green fluorescence. The results obtained from the amoebae treated with the COVID Box agents (Fig. 5D–O) were corroborated by the positive control, amphotericin B (Fig. 5P–R), where green fluorescence emission was also shown. ANOVA was used to assess differences among the values, indicating substantial contrasts (****$p <$ 0.0001) in the comparison between the treated and non-treated cells.

3.3.4. Inhibition of ATP production

An additional indicator of mitochondrial damage is a significant decrease in ATP production. To measure ATP levels, the Cell Titer-Glo® Luminescent Cell Viability Assay kit (Promega Biotech Ibérica, Madrid, Spain) was used. The results are depicted in a bar graph (Fig. 6), illustrating the inhibition of ATP synthesis in treated amoebae with these chemicals. Moreover, the significant damage inflicted by clemastine on the mitochondria is emphasized, able to inhibit over 96% of ATP synthesis in comparison to the negative control (non-treated cells). This inhibition result is similar to that obtained in treated cells with the reference compound amphotericin B (>98%). Furthermore, the significance of this decrease was confirmed by the ANOVA (****$p < 0.0001$), thus validating the mitochondrial damage.

3.3.5. ROS overproduction identification

To detect this ROS accumulation, CellROX Deep Red fluorescent kit (Thermo Fisher Scientific, Madrid, Spain) was used. In the negative control (Fig. 7 A, B), untreated amoebae, internal defense and repair mechanisms counteract any potential oxidative stress, making the generated ROS either non-visible or barely visible under the inverted fluorescence microscope. On the other hand, in treated trophozoites with COVID Box products (Fig. 7C–J), red fluorescence emission occurs due to the accumulation of these species, indicating increased cellular stress. The results of the drugs under evaluation were compared to those obtained from our positive control (Fig. 7 K, L), where a similar fluorescence pattern was observed. Differences between the values were assessed using a one-way analysis of variance (ANOVA). The results displayed significant differences (****$p < 0.0001$) when comparing treated cells to the negative controls.

4. Discussion

The urgent need for novel therapies against *Naegleria fowleri* emphasizes the persistent challenges posed by this neglected pathogen. With limited attention from pharmaceutical companies coupled with

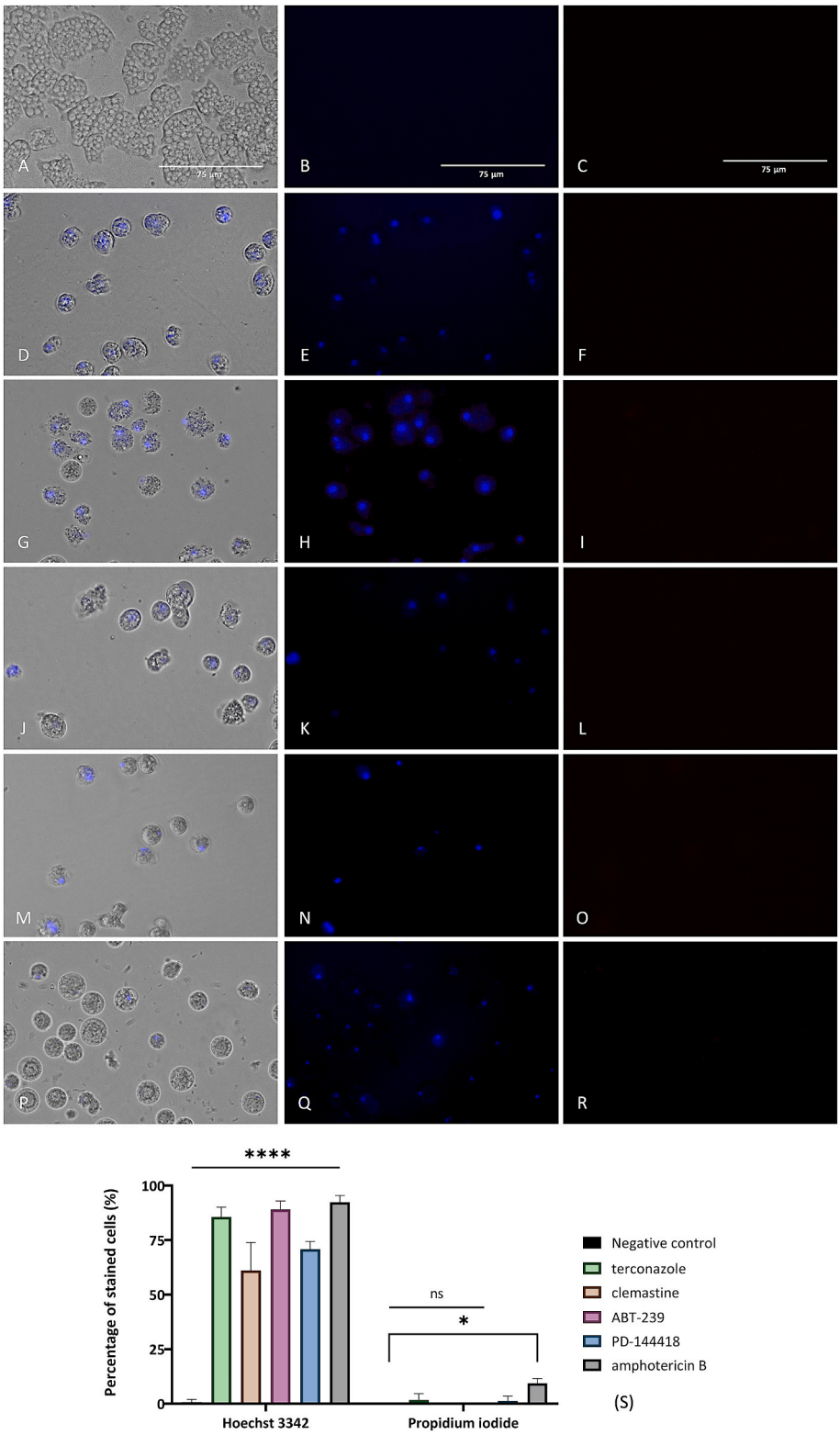

Fig. 3. Double staining kit (Hoechst 33342/PI) for the analysis of chromatin condensation. Negative control (A–C), terconazole (D–F), clemastine (G–I), ABT-239 (J–L), PD-144418 (M–O) and amphotericin B (P–R). Notably, all treated amoebae with an IC_{90} of the respective molecules exhibited blue fluorescence (B, E, H, K, N, Q). Additionally, after 24 h, no red fluorescence was observed, indicating that the amoebae were in an early stage of apoptosis. A negative control was used as a reference of healthy cells. Amphotericin B served as a reference compound for evaluating its effects against amoebae in comparison to the test compounds. All images were taken at the same time with 3 different visible/fluorescent channels with a thickness of 40x. An EVOS™ M5000 Cell Imaging System, Life Technologies, Madrid, Spain was used to capture the images. Scale bar: 75 µm. The bar graph (S) presents the percentage of cells that emit blue and red fluorescence post-incubation with the dyes. The data represents the mean values from three separate assays, along with the standard deviation (SD). A one-way analysis of variance (ANOVA) was also assessed to determine the statistical differences between the treated cells and the negative control, $*p < 0.05$; $****p < 0.0001$; ns = not significant. Each counting involved the analysis of three different pictures using the EVOS™ M5000 software tools.

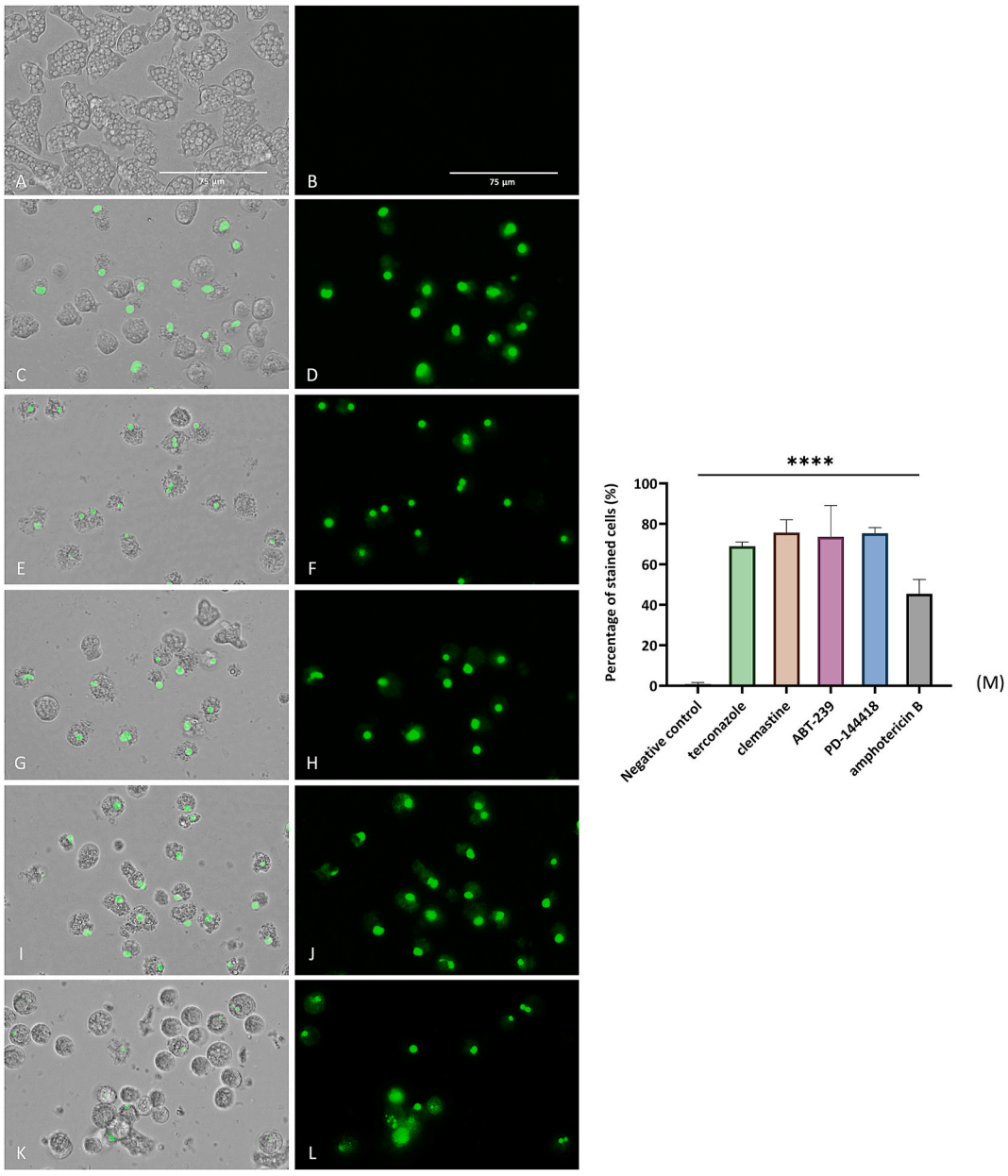

Fig. 4. Increase of plasma membrane permeability determined by SYTOX™ Green reagent. Negative control (A–B), terconazole (C–D), clemastine (E–F), ABT-239 (G–H), PD-144418 (I–J) and amphotericin B (K–L). All treated amoebae with an IC_{90} of compounds exhibited green fluorescence (B, E, H, K, N, Q), indicating enhanced membrane permeability, facilitating the ingress of the reagent and its binding to nucleic acids. A negative control served as a reference for healthy cells, demonstrating impermeability to the utilized reagent. Amphotericin B was utilized as a reference compound to assess its effects on amoebae in comparison to the evaluated compounds. All images were captured simultaneously using distinct (Overlay/GFP) channels at 40x. An EVOS™ M5000 Cell Imaging System, Life Technologies, Madrid, Spain was used to capture the images. Scale bar: 75 µm. In the bar graph (M), the mean value ± SD of green fluorescence-stained amoebae and the negative control was displayed. A one-way analysis of variance (ANOVA) was conducted to assess the statistical variances between the treated cells and the negative control. Statistical significance was represented as follows: $^{**}p < 0.01$; $^{***}p < 0.001$; $^{****}p < 0.0001$; ns = not significant. Three separate images were analyzed using the EVOS™ M5000 software, for each count.

limited research and divulgation, the development of effective treatments for diseases caused by *N. fowleri* remains a serious unmet requirement. Within this research context, our principal aim was to identify compounds, sourced from the COVID-Box, capable of effectively combat *N. fowleri* and potentially serve as the foundation for future chemicals development. This approach led to the discovery of four promising molecules namely terconazole, clemastine, ABT-239, and PD-144418. These active compounds demonstrated promising inhibitory effects against *N. fowleri*, showing an in vitro IC_{50} value of 1.96 ± 0.60 µM in parasite viability (ATCC® 30,808™) upon exposure to terconazole, IC_{50} of 7.68 ± 0.32 µM with clemastine, IC_{50} of 3.65 ± 0.79 µM with ABT-239, and IC_{50} 4.71 ± 0.95 µM with PD-144418. In addition, the effect of these compounds against the resistance phase of the parasite was also demonstrated. This, coupled with a cytotoxic concentration ranging from 48 to 84 µM among the compounds, results in all of them achieving a selectivity index higher than the one obtained for some certain reference drugs such as miltefosine (see Table 1).

Moreover, considering the broad-spectrum activity of the evaluated compounds, they are likely to demonstrate significant efficacy against a variety of other pathogenic microorganisms. Terconazole, recognized for its antifungal properties, has exhibited notable activity against Candida albicans and Candida glabrata (Sood et al., 2000; Spitzer and

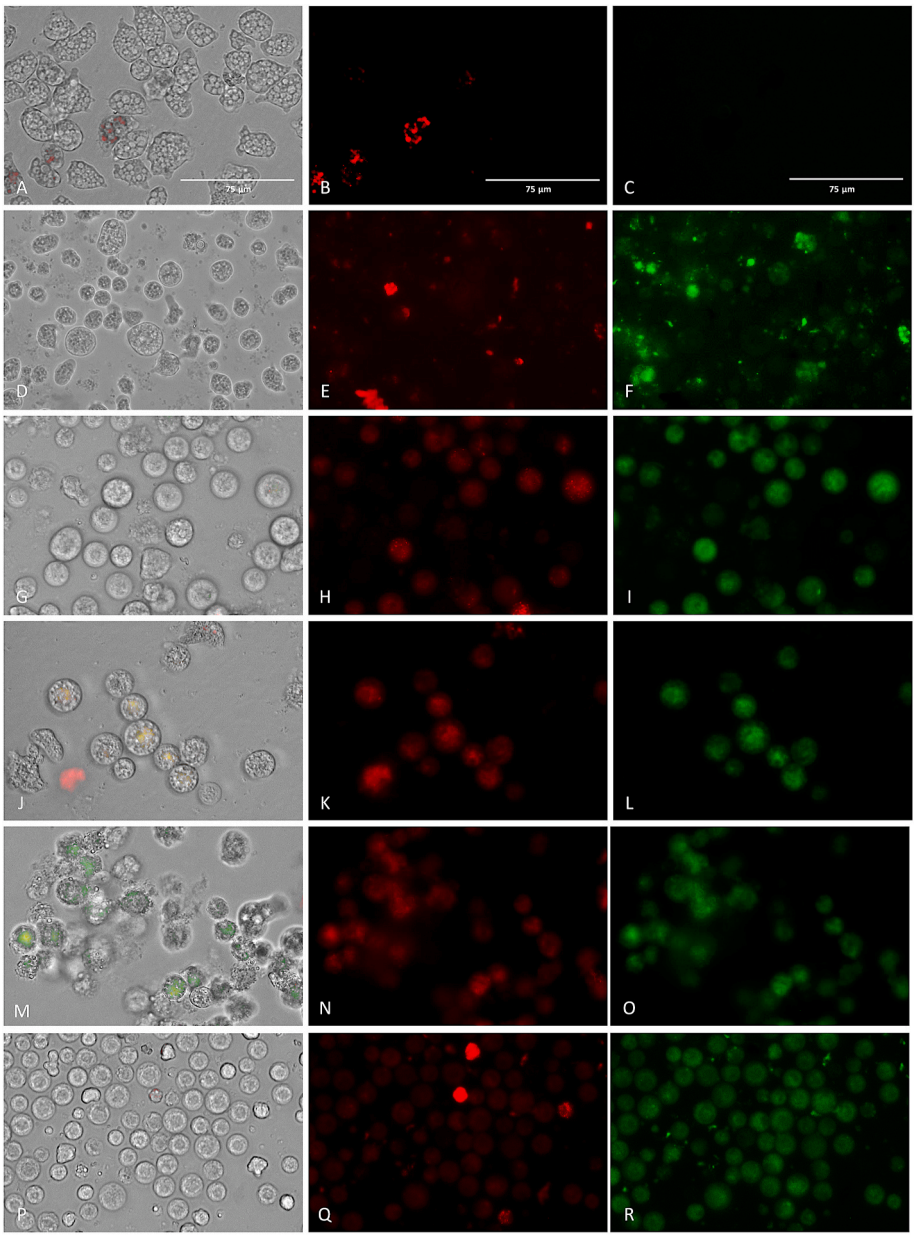

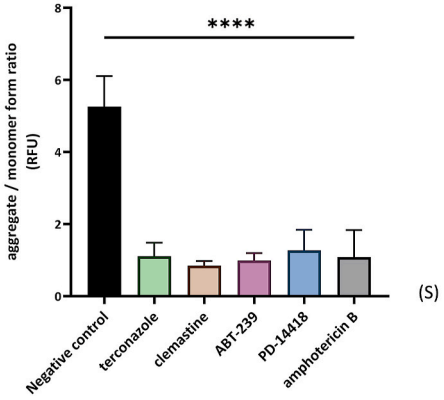

(caption on next page)

Fig. 5. JC-1 manifests the mitochondrial membrane potential depolarization. Negative control (A–C), terconazole (D–F), clemastine (G–I), ABT-239 (J–L), PD-144418 (M–O) and amphotericin B (P–R). All treated amoebae with an IC_{90} of molecules exhibited green (C, F, I, L, O, R) and red fluorescence (B, E, H, K, N, Q), indicating a decline in mitochondrial membrane potential. A negative control was used as a reference for healthy cells. Treated trophozoites with amphotericin B at IC_{90} served as a positive control. All images were captured simultaneously using three different (Overlay/RFP/GFP) channels at 40× magnification, employing an EVOS™ M5000 Cell Imaging System, Life Technologies, Madrid, Spain. Scale bar: 75 μm. The bar graph (S) illustrates the percentage of cells emitting green and red fluorescence after incubation with the dyes. Data represent the mean values ± SD of three different assays. A one-way analysis of variance (ANOVA) was also assessed to determine the statistical differences between the treated cells and the negative control, $^{**}p < 0.01$; $^{***}p < 0.001$; $^{****}p < 0.0001$; ns = not significant. For each counting, three different pictures were analyzed in the EVOS™ M5000 Cell Imaging System software, Life Technologies.

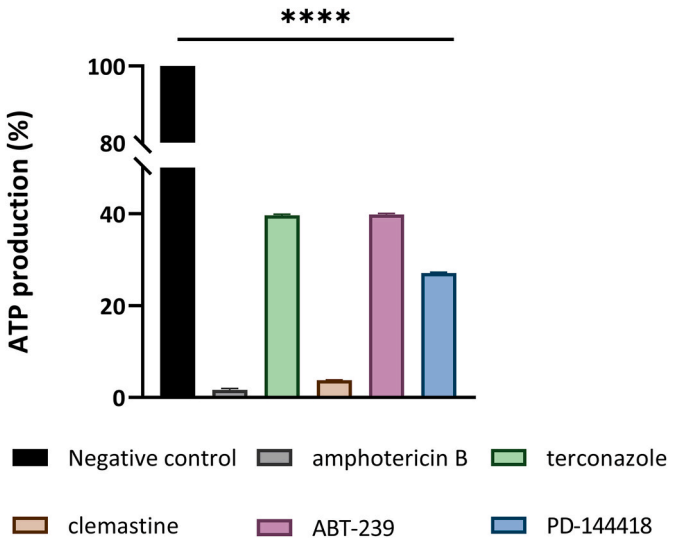

Fig. 6. ATP production was measured by Cell Titer-Glo®. Non-treated amoebae were used as negative control. Treated trophozoites with Amphotericin B IC_{90} was carried out as a positive control. All treated trophozoites with IC_{90} of COVID Box compounds displayed a significative decrease in ATP levels compared with Negative control. Data represent the mean values of three different assays and the standard deviation (SD). A one-way analysis of variance (ANOVA) was also assessed to determine the statistical differences between the treated cells and the negative control, $^{****}p < 0.0001$.

Wiederhold, 2018), as well as against the protozoa Trypanosoma cruzi (Reigada et al., 2019). This molecule that belongs to the group of azoles, acts by inhibiting the 14-alpha-demethylase, a key enzyme for the ergosterol biosynthesis (Zarn et al., 2003) that has been demonstrated as an essential lipid for the *N. fowleri* trophozoite's survival (Zhou et al., 2018). In fact, compounds that bind to the ergosterol or inhibit its synthesis are already used to treat *N. fowleri* infections, like amphotericin B and fluconazole (Hahn et al., 2020; Pugh and Levy, 2016).

Clemastine, in addition to its antihistamine effects (Herman and Vender, 2003), is another of the compounds that have shown anti-viral activity against respiratory viruses, in specific SARS-CoV-2 (Sauvat et al., 2020). Moreover, it has also shown antiprotozan activity against the parasites of the apicomplexa group, Toxoplasma gondii and Plasmodium spp. (Abbaali et al., 2021). The mechanism of action of clemastine in protozoa relies on its bind and destabilization of the TRiC/CCT chaperonin (Abbaali et al., 2021; Lu et al., 2020). This heterooligomeric complex is required for the folding of the cytoskeletal proteins actin and tubulin, which are part of the microfilaments and microtubules of the cells, as well as been involved in the cell division (Grantham, 2020; Wang et al., 2020).

ABT-239 is a potent H3 histamine receptor antagonist. These molecules are related to the treatment of different cognitive disorders such as schizophrenia or Alzheimer (Esbenshade et al., 2008; Fox et al., 2005). Since the H3 histamine receptor is located in the CNS (Schlicker and Kathmann, 2017), the cross of the blood brain barrier (BBB) would not represent any issue for the treatment and elimination of the amoebae in the brain. In fact, this is one of the most common obstacles in the search of new molecules to fight the PAM. This work represents the first report of the biological activity against a microorganism.

PD-144418 is a highly affinity, potent and selective sigma 1 (σ1) receptor ligand with antiviral activity (Gordon et al., 2020). On the other hand, recently, the similarity between the σ1 brain receptor and the catalytic domain of ERG2 has been described, sharing 30% sequence identity and 60% sequence homology (Shi et al., 2019). This enzyme is considered as a potential therapeutic target against *N. fowleri* since it is involved in the ergosterol biosynthesis. Having this in mind, some authors have proposed the non-opioid σ1 receptor as new target to find novel molecules with anti-*Naegleria* activity (Zhou et al., 2018). The great activity of the PD-144418 against two different strains of *N. fowleri* described in this work is aligned with the previous statement. These results demonstrate that these compounds can combat several infections and contribute to the effective treatment of a wide range of diseases.

The compounds to be considered as alternative therapeutic option against PAM, must induce a controlled death of the parasite, by triggering a programmed cell death (PCD) process in the parasite. In this context, our study focused on investigating PCD induction, emphasizing the identification of key metabolic events crucial for pathogen elimination without compromising the patient's well-being. Recognizable features associated with PCD induction include chromatin condensation, alterations in plasma membrane permeability, increased ROS production and a decrease of the mitochondrial membrane potential. These events suggest the activation of specific PCD pathways, which can trigger the regulated elimination of *Naegleria fowleri* trophozoites. On the other hand, inducing a non-regulated cell death, often marked by the absence of typical apoptotic or autophagic features, may trigger inflammatory processes, exacerbating the disease's pathogenesis and hastening the patient's demise.

Fundings

This work was funded by the Consorcio Centro de Investigación Biomédica (CIBER) de Enfermedades Infecciosas (CIBERINFEC); Instituto de Salud Carlos III, 28,006 Madrid, Spain (CB21/13/00100); and Cabildo Insular de Tenerife 2023–2028 and Ministerio de Sanidad, Spain. J.C.P. and I.S. were funded by the Cabildo Insular de Tenerife 2023–2028 (PROYECTO CC20230222, CABILDO.23). I.A.J. (TESIS, 2020010063) was funded by a grant from the Agencia Canaria de Investigación, Innovación y Sociedad de la Información, cofunded with 85% by FSE.

CRediT authorship contribution statement

Javier Chao-Pellicer: Writing – original draft, Software, Methodology, Investigation, Data curation. **Iñigo Arberas-Jiménez:** Writing – original draft, Software, Methodology, Investigation, Data curation. **Ines Sifaoui:** Software, Methodology, Investigation, Data curation. **José E. Piñero:** Writing – review & editing, Visualization, Validation, Supervision, Resources, Project administration, Funding acquisition, Formal analysis, Conceptualization. **Jacob Lorenzo-Morales:** Writing – review & editing, Visualization, Validation, Supervision, Resources, Project administration, Funding acquisition, Formal analysis, Conceptualization.

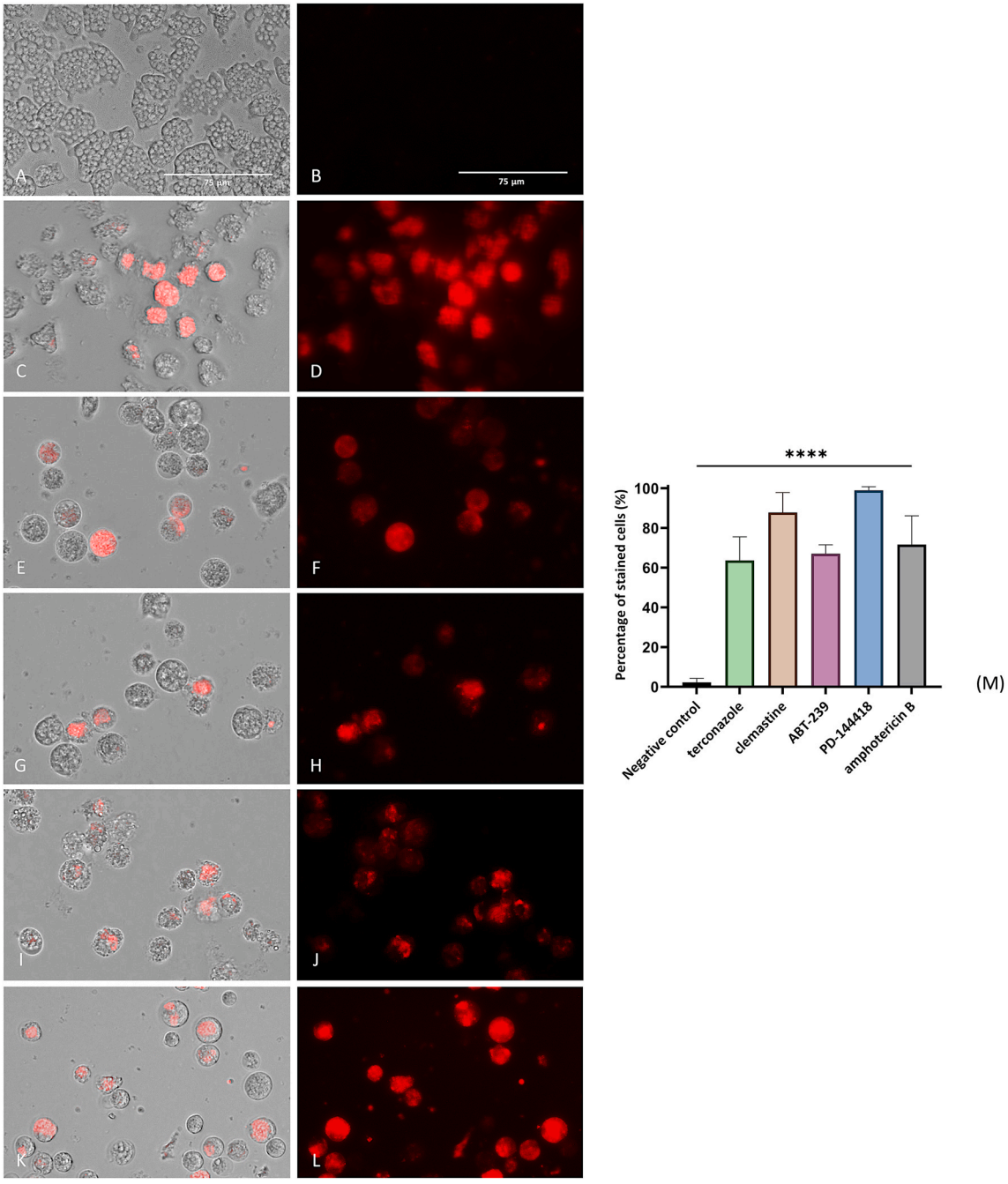

Fig. 7. ROS overproduction was detected using CellROX Deep Red fluorescent kit. Negative control (A–B), terconazole (C–D), clemastine (E–F), ABT-239 (G–H), PD-144418 (I–J) and amphotericin B (K–L). All treated amoebae with an IC_{90} of compounds exhibited red fluorescence (B, E, H, K, N, Q), indicating an increase in the formation of ROS. A negative control served as a reference for healthy cells, with lower levels of ROS, barely showing any fluorescence. The effects of the treated amoebae were compared with a positive control, the reference drug amphotericin B. The images were all captured at the same time, employing separate Overlay/GFP channels at 40× magnification. For capturing the images, EVOS™ M5000 Cell Imaging System, Life Technologies, Madrid, Spain was used. Scale bar: 75 µm. In the bar graph (M), the mean value ± SD of amoebae of stained cells and negative control was presented. An analysis of the statistical variances between the treated and non-treated cells was conducted through a one-way analysis of variance (ANOVA). Representation of statistical significance was as follows: ****$p < 0.0001$; ns = not significant. Each count involved the analysis of three separate images using the EVOS™ M5000 software.

Declaration of competing interest

The authors declare that they have no known competing financial interests or personal relationships that could have appeared to influence the work reported in this paper.

Acknowledgements

Authors would like to thank Medicines for Malaria Venture (MMV, Geneva, Switzerland) for providing the COVID box.

Appendix A. Supplementary data

Supplementary data to this article can be found online at https://doi.

org/10.1016/j.ijpddr.2024.100545.

References

Abbaali, I., Truong, D.A., Day, S.D., Haro-Ramirez, N., Morrissette, N.S., 2021. Systematic analysis of clemastine, a candidate apicomplexan parasite-selective tubulin-targeting agent. Int. J. Mol. Sci. 23 https://doi.org/10.3390/ijms23010068.

Almeida-Paes, R., de Andrade, I.B., Ramos, M.L.M., Rodrigues, M.V. de A., do Nascimento, V.A., Bernardes-Engemann, A.R., Frases, S., 2021. Medicines for Malaria Venture COVID Box: a source for repurposing drugs with antifungal activity against human pathogenic fungi. Mem. Inst. Oswaldo Cruz 116, e210207. https://doi.org/10.1590/0074-02760210207.

Arberas-Jiménez, I., Rizo-Liendo, A., Sifaoui, I., Chao-Pellicer, J., Piñero, J.E., Lorenzo-Morales, J., 2022. A Fluorometric assay for the in vitro evaluation of activity against naegleria fowleri cysts. Microbiol. Spectr. 10, e0051522 https://doi.org/10.1128/spectrum.00515-22.

Baig, A.M., 2016. Primary amoebic meningoencephalitis: Neurochemotaxis and Neurotropic preferences of naegleria fowleri. ACS Chem. Neurosci. 7, 1026–1029. https://doi.org/10.1021/acschemneuro.6b00197.

Bellini, N.K., Santos, T.M., da Silva, M.T.A., Thiemann, O.H., 2018. The therapeutic strategies against Naegleria fowleri. Exp. Parasitol. 187, 1–11. https://doi.org/10.1016/j.exppara.2018.02.010.

Chang, W.-L., Hsu, L.-C., Leu, W.-J., Chen, C.-S., Guh, J.-H., 2015. Repurposing of nitroxoline as a potential anticancer agent against human prostate cancer: a crucial role on AMPK/mTOR signaling pathway and the interplay with Chk2 activation. Oncotarget 6, 39806–39820. https://doi.org/10.18632/oncotarget.5655.

Cope, J.R., Ratard, R.C., Hill, V.R., Sokol, T., Causey, J.J., Yoder, J.S., Mirani, G., Mull, B., Mukerjee, K.A., Narayanan, J., Doucet, M., Qvarnstrom, Y., Poole, C.N., Akingbola, O.A., Ritter, J.M., Xiong, Z., da Silva, A.J., Roellig, D., Van Dyke, R.B., Stern, H., Xiao, L., Beach, M.J., 2015. The first association of a primary amebic meningoencephalitis death with culturable Naegleria fowleri in tap water from a US treated public drinking water system. Clin. Infect. Dis. an Off. Publ. Infect. Dis. Soc. Am. 60, e36–e42. https://doi.org/10.1093/cid/civ017.

De Jonckheere, J.F., 2011. Origin and evolution of the worldwide distributed pathogenic amoeboflagellate Naegleria fowleri. Infect. Genet. Evol. J. Mol. Epidemiol. Evol. Genet. Infect. Dis. 11, 1520–1528. https://doi.org/10.1016/j.meegid.2011.07.023.

Dunn, A.L., Reed, T., Stewart, C., Levy, R.A., 2016. Naegleria fowleri that induces primary amoebic meningoencephalitis: rapid diagnosis and rare case of survival in a 12-Year-Old Caucasian Girl. Lab. Med. 47, 149–154. https://doi.org/10.1093/labmed/lmw008.

Dunnebacke, T.H., Schuster, F.L., Yagi, S., Booton, G.C., 2004. Balamuthia mandrillaris from soil samples. Microbiology 150, 2837–2842. https://doi.org/10.1099/mic.0.27218-0.

El Saftawy, E., Farag, M.F., Gebreil, H.H., Abdelfatah, M., Aboulhoda, B.E., Alghamdi, M., Albadawi, E.A., Abd Elkhalek, M.A., 2024. Malaria: biochemical, physiological, diagnostic, and therapeutic updates. PeerJ 12, e17084. https://doi.org/10.7717/peerj.17084.

Esbenshade, T.A., Browman, K.E., Bitner, R.S., Strakhova, M., Cowart, M.D., Brioni, J.D., 2008. The histamine H3 receptor: an attractive target for the treatment of cognitive disorders. Br. J. Pharmacol. 154, 1166–1181. https://doi.org/10.1038/bjp.2008.147.

Fox, G.B., Esbenshade, T.A., Pan, J.B., Radek, R.J., Krueger, K.M., Yao, B.B., Browman, K. E., Buckley, M.J., Ballard, M.E., Komater, V.A., Miner, H., Zhang, M., Faghih, R., Rueter, L.E., Bitner, R.S., Drescher, K.U., Wetter, J., Marsh, K., Lemaire, M., Porsolt, R.D., Bennani, Y.L., Sullivan, J.P., Cowart, M.D., Decker, M.W., Hancock, A. A., 2005. Pharmacological properties of ABT-239 [4-(2-{2-[(2R)-2-Methylpyrrolidinyl]ethyl}-benzofuran-5-yl)benzonitrile]: II. Neurophysiological characterization and broad preclinical efficacy in cognition and schizophrenia of a potent and selective histamine H3 r. J. Pharmacol. Exp. Ther. 313, 176–190. https://doi.org/10.1124/jpet.104.078402.

Gordon, D.E., Jang, G.M., Bouhaddou, M., Xu, J., Obernier, K., White, K.M., O'Meara, M. J., Rezelj, V.V., Guo, J.Z., Swaney, D.L., Tummino, T.A., Hüttenhain, R., Kaake, R. M., Richards, A.L., Tutuncuoglu, B., Foussard, H., Batra, J., Haas, K., Modak, M., Kim, M., Haas, P., Polacco, B.J., Braberg, H., Fabius, J.M., Eckhardt, M., Soucheray, M., Bennett, M.J., Cakir, M., McGregor, M.J., Li, Q., Meyer, B., Roesch, F., Vallet, T., Mac Kain, A., Miorin, L., Moreno, E., Naing, Z.Z.C., Zhou, Y., Peng, S., Shi, Y., Zhang, Z., Shen, W., Kirby, I.T., Melnyk, J.E., Chorba, J.S., Lou, K., Dai, S.A., Barrio-Hernandez, I., Memon, D., Hernandez-Armenta, C., Lyu, J., Mathy, C.J.P., Perica, T., Pilla, K.B., Ganesan, S.J., Saltzberg, D.J., Rakesh, R., Liu, X., Rosenthal, S.B., Calviello, L., Venkataramanan, S., Liboy-Lugo, J., Lin, Y., Huang, X.-P., Liu, Y., Wankowicz, S.A., Bohn, M., Safari, M., Ugur, F.S., Koh, C., Savar, N.S., Tran, Q.D., Shengjuler, D., Fletcher, S.J., O'Neal, M.C., Cai, Y., Chang, J. C.J., Broadhurst, D.J., Klippsten, S., Sharp, P.P., Wenzell, N.A., Kuzuoglu-Ozturk, D., Wang, H.-Y., Trenker, R., Young, J.M., Cavero, D.A., Hiatt, J., Roth, T.L., Rathore, U., Subramanian, A., Noack, J., Hubert, M., Stroud, R.M., Frankel, A.D., Rosenberg, O. S., Verba, K.A., Agard, D.A., Ott, M., Emerman, M., Jura, N., von Zastrow, M., Verdin, E., Ashworth, A., Schwartz, O., d'Enfert, C., Mukherjee, S., Jacobson, M., Malik, H.S., Fujimori, D.G., Ideker, T., Craik, C.S., Floor, S.N., Fraser, J.S., Gross, J. D., Sali, A., Roth, B.L., Ruggero, D., Taunton, J., Kortemme, T., Beltrao, P., Vignuzzi, M., García-Sastre, A., Shokat, K.M., Shoichet, B.K., Krogan, N.J., 2020. A SARS-CoV-2 protein interaction map reveals targets for drug repurposing. Nature 583, 459–468. https://doi.org/10.1038/s41586-020-2286-9.

Grace, E., Asbill, S., Virga, K., 2015. Naegleria fowleri: pathogenesis, diagnosis, and treatment options. Antimicrob. Agents Chemother. 59, 6677–6681. https://doi.org/10.1128/AAC.01293-15.

Grantham, J., 2020. The molecular Chaperone CCT/TRiC: an essential component of Proteostasis and a potential Modulator of protein aggregation. Front. Genet. 11, 172. https://doi.org/10.3389/fgene.2020.00172.

Güémez, A., García, E., 2021. Primary amoebic meningoencephalitis by naegleria fowleri: pathogenesis and treatments. Biomolecules 11. https://doi.org/10.3390/biom11091320.

Hahn, H.J., Abagyan, R., Podust, L.M., Roy, S., Ali, I.K.M., Debnath, A., 2020. HMG-CoA Reductase Inhibitors as drug leads against naegleria fowleri. ACS Chem. Neurosci. 11, 3089–3096. https://doi.org/10.1021/acschemneuro.0c00428.

Heggie, T.W., Küpper, T., 2017. Surviving Naegleria fowleri infections: a successful case report and novel therapeutic approach. Trav. Med. Infect. Dis. 16, 49–51. https://doi.org/10.1016/j.tmaid.2016.12.005.

Herman, S.M., Vender, R.B., 2003. Antihistamines in the treatment of dermatitis. J. Cutan. Med. Surg. 7, 467–473. https://doi.org/10.1007/s10227-003-0164-3.

Jahangeer, M., Mahmood, Z., Munir, N., Waraich, U.-E.-A., Tahir, I.M., Akram, M., Ali Shah, S.M., Zulfqar, A., Zainab, R., 2020. Naegleria fowleri: Sources of infection, pathophysiology, diagnosis, and management; a review. Clin. Exp. Pharmacol. Physiol. 47, 199–212. https://doi.org/10.1111/1440-1681.13192.

Jain, R., Prabhakar, S., Modi, M., Bhatia, R., Sehgal, R., 2002. Naegleria meningitis: a rare survival. Neurol. India 50, 470–472.

Kemble, S.K., Lynfield, R., DeVries, A.S., Drehner, D.M., Pomputius, W.F. 3rd, Beach, M. J., Visvesvara, G.S., da Silva, A.J., Hill, V.R., Yoder, J.S., Xiao, L., Smith, K.E., Danila, R., 2012. Fatal Naegleria fowleri infection acquired in Minnesota: possible expanded range of a deadly thermophilic organism. Clin. Infect. Dis. an Off. Publ. Infect. Dis. Soc. Am. 54, 805–809. https://doi.org/10.1093/cid/cir961.

Laniado-Laborín, R., Cabrales-Vargas, M.N., 2009. Amphotericin B: side effects and toxicity. Rev. Iberoam. De. Micol. 26, 223–227. https://doi.org/10.1016/j.riam.2009.06.003.

Lee, J., Kim, J.-H., Sohn, H.-J., Yang, H.-J., Na, B.-K., Chwae, Y.-J., Park, S., Kim, K., Shin, H.-J., 2014. Novel cathepsin B and cathepsin B-like cysteine protease of Naegleria fowleri excretory-secretory proteins and their biochemical properties. Parasitol. Res. 113, 2765–2776. https://doi.org/10.1007/s00436-014-3936-3.

Linam, W.M., Ahmed, M., Cope, J.R., Chu, C., Visvesvara, G.S., da Silva, A.J., Qvarnstrom, Y., Green, J., 2015. Successful treatment of an adolescent with Naegleria fowleri primary amebic meningoencephalitis. Pediatrics 135, e744–e748. https://doi.org/10.1542/peds.2014-2292.

Lu, K.-Y., Quan, B., Sylvester, K., Srivastava, T., Fitzgerald, M.C., Derbyshire, E.R., 2020. Plasmodium chaperonin TRiC/CCT identified as a target of the antihistamine clemastine using parallel chemoproteomic strategy. Proc. Natl. Acad. Sci. U. S. A. 117, 5810–5817. https://doi.org/10.1073/pnas.1913525117.

Martínez, D.Y., Bravo-Cossio, F., Valdivia-Tapia, M.D.C., Carreazo, N.Y., Cabello-Vilchez, A.M., 2022. Successful treatment of primary amoebic meningoencephalitis using a novel therapeutic Regimen including miltefosine and voriconazole. Acta Parasitol. 67, 1421–1424. https://doi.org/10.1007/s11686-022-00591-9.

McBride, J., Ingram, P.R., Henriquez, F.L., Roberts, C.W., 2005. Development of colorimetric microtiter plate assay for assessment of antimicrobials against Acanthamoeba. J. Clin. Microbiol. 43, 629–634. https://doi.org/10.1128/JCM.43.2.629-634.2005.

Piñero, J.E., Chávez-Munguía, B., Omaña-Molina, M., Lorenzo-Morales, J., 2019. Naegleria fowleri. Trends Parasitol. 35, 848–849. https://doi.org/10.1016/j.pt.2019.06.011.

Pugh, J.J., Levy, R.A., 2016. Naegleria fowleri: diagnosis, pathophysiology of brain inflammation, and Antimicrobial treatments. ACS Chem. Neurosci. 7, 1178–1179. https://doi.org/10.1021/acschemneuro.6b00232.

Pushpakom, S., Iorio, F., Eyers, P.A., Escott, K.J., Hopper, S., Wells, A., Doig, A., Guilliams, T., Latimer, J., McNamee, C., Norris, A., Sanseau, P., Cavalla, D., Pirmohamed, M., 2019. Drug repurposing: progress, challenges and recommendations. Nat. Rev. Drug Discov. 18, 41–58. https://doi.org/10.1038/nrd.2018.168.

Reigada, C., Sayé, M., Valera-Vera, E., Miranda, M.R., Pereira, C.A., 2019. Repurposing of terconazole as an anti Trypanosoma cruzi agent. Heliyon 5, e01947. https://doi.org/10.1016/j.heliyon.2019.e01947.

Rizo-Liendo, A., Sifaoui, I., Reyes-Batlle, M., Chiboub, O., Rodríguez-Expósito, R.L., Bethencourt-Estrella, C.J., San Nicolás-Hernández, D., Hendiger, E.B., López-Arencibia, A., Rocha-Cabrera, P., Piñero, J.E., Lorenzo-Morales, J., 2019. Basel, Switzerland). https://doi.org/10.3390/pathogens8030122.

Rodríguez-Mera, I.B., Carrasco-Yépez, M.M., Vásquez-Moctezuma, I., Correa-Basurto, J., Salinas, G.R.-, Castillo-Ramírez, D.A., Rosales-Cruz, É., Rojas-Hernández, S., 2022. Role of cathepsin B of Naegleria fowleri during primary amebic meningoencephalitis. Parasitol. Res. 121, 3287–3303. https://doi.org/10.1007/s00436-022-07660-y.

Sauvat, A., Ciccosanti, F., Colavita, F., Di Rienzo, M., Castilletti, C., Capobianchi, M.R., Kepp, O., Zitvogel, L., Fimia, G.M., Piacentini, M., Kroemer, G., 2020. On-target versus off-target effects of drugs inhibiting the replication of SARS-CoV-2. Cell Death Dis. 11, 656. https://doi.org/10.1038/s41419-020-02842-x.

Schlicker, E., Kathmann, M., 2017. Role of the histamine H(3) receptor in the central nervous system. Handb. Exp. Pharmacol. 241, 277–299. https://doi.org/10.1007/164_2016_12.

Schumacher, D.J., Tien, R.D., Lane, K., 1995. Neuroimaging findings in rare amebic infections of the central nervous system. AJNR. Am. J. Neuroradiol. 16, 930–935.

Schuster, F.L., Guglielmo, B.J., Visvesvara, G.S., 2006. In-vitro activity of miltefosine and voriconazole on clinical isolates of free-living amebas: Balamuthia mandrillaris, Acanthamoeba spp., and Naegleria fowleri. J. Eukaryot. Microbiol. 53, 121–126. https://doi.org/10.1111/j.1550-7408.2005.00082.x.

Serrano-Luna, J., Cervantes-Sandoval, I., Tsutsumi, V., Shibayama, M., 2007. A biochemical comparison of proteases from pathogenic naegleria fowleri and non-

pathogenic Naegleria gruberi. J. Eukaryot. Microbiol. 54, 411–417. https://doi.org/10.1111/j.1550-7408.2007.00280.x.

Shi, D., Chahal, K.K., Oto, P., Nothias, L.-F., Debnath, A., McKerrow, J.H., Podust, L.M., Abagyan, R., 2019. Identification of four amoebicidal Nontoxic compounds by a molecular Docking screen of naegleria fowleri sterol Δ8-Δ7-Isomerase and Phenotypic assays. ACS Infect. Dis. 5, 2029–2038. https://doi.org/10.1021/acsinfecdis.9b00227.

Sood, G., Nyirjesy, P., Weitz, M.V., Chatwani, A., 2000. Terconazole cream for non-Candida albicans fungal vaginitis: results of a retrospective analysis. Infect. Dis. Obstet. Gynecol. 8, 240–243. https://doi.org/10.1155/S1064744900000351.

Spitzer, M., Wiederhold, N.P., 2018. Reduced antifungal Susceptibility of Vulvovaginal Candida species at normal Vaginal pH levels: clinical Implications. J. Low. Genit. Tract Dis. 22, 152–158. https://doi.org/10.1097/LGT.0000000000000383.

Wang, D.Y., Kamuda, K., Montoya, G., Mesa, P., 2020. The TRiC/CCT chaperonin and its role in Uncontrolled Proliferation. Adv. Exp. Med. Biol. 1243, 21–40. https://doi.org/10.1007/978-3-030-40204-4_2.

Zarn, J.A., Brüschweiler, B.J., Schlatter, J.R., 2003. Azole fungicides affect mammalian steroidogenesis by inhibiting sterol 14 alpha-demethylase and aromatase. Environ. Health Perspect. 111, 255–261. https://doi.org/10.1289/ehp.5785.

Zhou, W., Debnath, A., Jennings, G., Hahn, H.J., Vanderloop, B.H., Chaudhuri, M., Nes, W.D., Podust, L.M., 2018. Enzymatic chokepoints and synergistic drug targets in the sterol biosynthesis pathway of Naegleria fowleri. PLoS Pathog. 14, e1007245 https://doi.org/10.1371/journal.ppat.1007245.